Dalton Transactions

Accepted Manuscript

ROYAL SOCIETY OF CHEMISTRY

www.rsc.org/dalton

Graphical Abstract

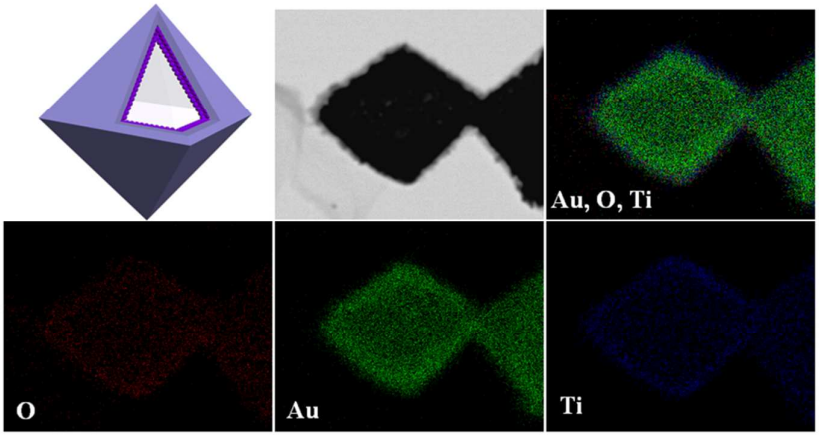

The gold@titanium dioxide octahedral nanocages (Au@TiO_2) with a well-defined double-shelled structure with Au as internal shell and TiO_2 as external shell exhibit excellent and stable activity for the catalytic reduction of 4-nitrophenol.

Cite this: DOI: 10.1039/c0xx00000x

www.rsc.org/xxxxxx

ARTICLE TYPE

Au@TiO_2 double-shelled octahedral nanocages with improved catalytic property†

Xiaoming Lv, Yihua Zhu,* Hongliang Jiang, Hua Zhong, Xiaoling Yang, and Chunzhong Li*

Received (in XXX, XXX) Xth XXXXXXXXX 20XX, Accepted Xth XXXXXXXXX 20XX

DOI: 10.1039/b000000x

A novel and facile strategy has been successfully developed to synthesize uniform gold@titanium dioxide octahedral nanocages (Au@TiO_2), which have a well-defined double-shelled structure with Au as internal shell and TiO_2 as external shell. The unique Au@TiO_2 double-shelled octahedral nanocages were elaborately fabricated by a Cu_2O-templated strategy combining with spatially confined galvanic replacement. The formation process of these delicate hierarchical octahedral architectures is discussed in detail. The catalytic performance of the Au@TiO_2 double-shelled octahedral nanocages was investigated using the reduction of 4-nitrophenol as a model reaction. The mesoporous structure of both the Au and TiO_2 shells provide direct access for the reactant molecules to diffuse and subsequently interact with the Au shell. This novel catalyst shows excellent and stable activity for the catalytic reduction of 4-nitrophenol, which can be recycled for ten successive cycles of the reaction with conversion efficiency of more than 90%. The superior catalytic activity attributes to mesoporous double shells, enhanced synergistic effects between the Au and TiO_2 shells, and unique properties of octahedral structure. More importantly, the as-obtained Au@TiO_2 double-shelled octahedral nanocages also show potential applications in solar cells, organocatalysis and water splitting.

1. Introduction

Hollow nanostructures have attracted tremendous attention over the past few decades because of their unique properties, such as designable morphology, low density, large void space, high surface area and shell permeability, which give them potential for applications in catalysis, delivery vehicles, photonic materials, optics, sensors, rechargeable batteries.[1-3] Specifically, anisotropic nanocages with non-spherical shapes and regular interiors are of particular interests for their fascinating advantages.[4-6] For instance, anisotropic cages are beneficial in biomedical applications,[5] targeted drug delivery,[6] and energy storage.[7] Their anisotropic features even offer them the possibility to be essential building blocks of complex hierarchical architectures with multiple functionalities.[8]

Noble metal nanocages are a class of most investigated materials for their unique properties and great importance in many advanced applications. For example, Fang et al. synthesized Au mesocages which show a strong shape effect in highly sensitive single-particle surface-enhanced Raman spectroscopy.[9] Xia et al. highlighted the photothermal properties of Au nanocages for both cancer diagnosis and treatment.[10] Mostafa et al. also found that the Au nanoparticles having sharp corners and edges have enhanced catalytic activity.[11] Up to now, noble metal nanocages have been synthesized by several groups[12-21] using Ag polyhedrons, Ag_2O, Co, Te, Ni or Cu_2O nanostructures as sacrificial templates via selective removal of the core from the core/shell structures. Although many advances for the synthesis and applications of hollow noble metal with controllable structures have been achieved, it still remains a problem that noble metal nanostructures tend to deform owing to their exposure to reactants and the surrounding medium, leading to rapid decay of catalytic activity and stability.[22] In addition, further functionalization of noble metal nanocages is urgently addressed.

It is generally accepted that core-shell nanostructure with the metal composite embedded inside an oxide matrix (e.g., SiO_2, TiO_2, CeO_2, ZrO_2) protects the former from agglomerating and getting exposed to the reactants and the surrounding medium.[23-27] In addition, the encapsulation also increases the contact area between the metal composite and the oxide matrix and therefore allows for stronger synergistic interactions between them.[28] Although it seems attractive that metal-oxide hollow polyhedral structures integrate the features of both a hollow interior and the novel properties arising from the combination of individual constituents, these reports on the synthesis of metal-oxide hetero-structural polyhedral cages are still lacking despite there are few examples of Au-CuO "microcage"[29] or Au@SiO_2 nanocage.[30,31] Therefore, exploration of the controllable synthesis of polyhedral hollow nanostructures of metal-oxide herero-structured materials is driven by both the synthetic challenges and the multi-functional properties of the products offered by their complex nanostructures.

In this work, we have prepared nano-sized Au@TiO_2 double-shelled octahedral nanocages using a Cu_2O-templated strategy

combining with spatially confined galvanic replacement. The controlled growth process of these hierarchical octahedral architectures is discussed. The produced octahedral Au@TiO_2 double-shelled nanocages possess unique structural features such as large surface area, highly roughened surface topography, enhanced synergistic effect, and decreased aggregation, leading to extremely high activity and stability. Finally, their catalytic performance towards the conversion of 4-nitrophenol (4-NP) to 4-aminophenol (4-AP) by $NaBH_4$ as a model reaction was also investigated. Interestingly, it was found that the Au@TiO_2 double-shelled nanocages show excellent catalytic ability and is more stable compared to the bare Au nanocages, which allows it to be reused over multiple cycles while maintaining its catalytic activity.

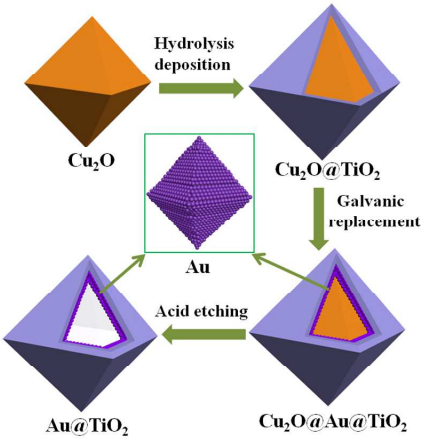

Scheme 1. Schematic diagram of the fabrication of Au@TiO_2 double-shelled octahedral nanocages.

2. Experimental

2.1. Reagents and Materials

Poly(vinyl pyrrolidone) (PVP, M_w = 40000) and Titanium tetrafluoride (TiF_4) was purchased from Sigma-Aldrich. Copper chloride dehydrate ($CuCl_2{\cdot}2H_2O$), Gold chloride trihydrate ($HAuCl_4{\cdot}3H_2O$), sodium citrate ($C_6H_5O_7Na_3{\cdot}2H_2O$), glucose ($C_6H_{12}O_6$) sodium hydroxide (NaOH), nitric acid (HNO_3) were all obtained from Shanghai Lingfeng Chemical Reagent Co. All the chemicals were used as received. All aqueous solutions were prepared using deionized (DI) water with a resistivity of 18 MΩ·cm.

2.2. Synthesis of Cu_2O precursor templates

Cu_2O precursor octahedras were synthesized by a modified method as described in Lou's work.[32] In a typical procedure, 10 mL of an aqueous solution of NaOH (2 M) was added dropwise into 100 mL of a mixture solution containing $CuCl_2{\cdot}2H_2O$ (10 mM), sodium citrate (3.4 mM) and PVP (M_w = 40000, 0.04 g mL^{-1}) under stirring. After 0.5 h, 10 mL of an ascorbic acid solution (0.6 M) was added dropwise into the above solution. The resultant suspension was further aged at 33 ºC for 2.5 h to produce Cu_2O octahedral with edge length of 250 nm.

2.3. Synthesis of Cu_2O@TiO_2 core/shell structure

In a typical procedure, 0.01 g of Cu_2O templates was dispersed into 25 mL of de-ionized (DI) water by ultra-sonication, followed by addition of 0.6 mL of an aqueous solution of TiF_4 (0.02 M). After thorough mixing, the suspension was transferred into a 50 mL Teflon-lined stainless steel autoclave and heated at 180 ºC for 1 h. After the reaction, the products were harvested by several rinse-centrifugation cycles with DI water and ethanol for further characterization.

2.4. Synthesis of Au@TiO_2 double-shelled structure

In a typical procedure, 10 mg of the produced Cu_2O@TiO_2 materials were dispersed in H_2O containing 1 % PVP (M_w = 40000). After 10 min constant stirring, the mixture was heated to 60 ºC,[20] 1.5 mL various concentration of $HAuCl_4$ solution from 5 mM to 30 mM was added to the stirred solution. The solution turned black at the beginning a few minutes, suggesting the formation of Cu_2O@Au@TiO_2 core shell nanostructure. These Cu_2O@Au@TiO_2 core shell particles were then immersed in a 1 % PVP (Mw = 40000) and 0.15 M HNO_3 solution for 12 h to remove the inner Cu_2O core. The precipitates were separated by centrifugation, washed with DI water and ethanol, and dried under vacuum overnight.

2.5. Synthesis of Au nanocages

For the synthesis of Au nanocages, most of the procedure is the same as the procedure for preparing the Au@TiO_2 structure except that the 10 mg of Cu_2O@TiO_2 materials were replaced by 10 mg of Cu_2O templates. The precipitates were separated by centrifugation, washed with DI water and ethanol, and dried under vacuum overnight.

2.6. Synthesis of Au nanoparticles

Au nanoparticles were synthesized by the similar method to preparation of Au nanocages but without the addition of PVP. The precipitates were separated by centrifugation, washed with DI water and ethanol, and dried under vacuum overnight.

2.7. Measurements and Characterizations

The morphology and microstructure of all samples were examined by High-transmission electron microscopy (TEM: JEM-2100, operated at 200kV) equipped with an energy dispersive X-ray analyzer (EDX) and Scanning electron microscopy (FE-SEM: S-4800). X-ray power diffraction (RIGAK, D/MAX 2550 VB/PC, Japan) was used for crystalline structure. The UV-visible absorption spectra were recorded with a UV-vis spectrometer (UNICO UV-2102PC) at 25 ºC. Brunauer-Emmett-Teller (BET) and Barrett-Joyner-Halenda (BJH) models were used to determine the specific surface areas, pore volume, and the pore sizes of the samples, respectively. Inductively coupled plasma atomic emission spectroscopy (ICP-AES) was carried out in SHIMADZU ICPS-8100.

2.8. Catalytic performance measurement

The catalysis experiments were carried out in a 50 mL long neck quartz cuvette. Typically, a certain amount of the catalyst was dispersed in 10 mL DI water, 1 mL of the catalyst solution was added into 24 mL of a mixture solution containing 4-nitrophenol (10^{-4} M) and sodium borohydride (0.3 M) under stirring at room temperature. UV-Vis spectra were recorded every 1 min to monitor the progress of the reaction. Once the reaction was completed, the catalyst was separated by centrifugation and

washed with deionized water. The separated catalyst was then reused to initiate the second cycle of the reaction. The same procedure was performed repeatedly several times. Actually, as the reaction proceeds, one could observe the gradual change of the solution colour from yellow to colourless. The use of an excess of $NaBH_4$ ensures that its concentration remains essentially constant during the reaction, which allows the assumption of pseudo-first-order kinetics with respect to nitro compound.

3. Results and discussion

The synthesis strategy of $Au@TiO_2$ double-shelled octahedral nanocages is illustrated in Scheme 1. In the first step, highly uniform Cu_2O octahedral crystals were synthesized by reducing a copper-citrate complex solution with ascorbic acid in the presence of polyvinylpyrrolidone (PVP).[32] Afterward, a thin TiO_2 layer was preferentially deposited onto the Cu_2O due to the high activity of Cu_2O cores and accelerated hydrolysis of TiF_4, as described in Lou's work. Subsequently, the $Au@TiO_2$ nanocage was fabricated by a spatially confined galvanic replacement between the obtained $Cu_2O@TiO_2$ and $HAuCl_4$ according to a controllable strategy.

Figure 1 presents typical SEM and TEM images of the obtained Cu_2O and $Cu_2O@TiO_2$. The Cu_2O presents uniform octahedral structure with edge length of ca. 250 nm, as shown in Figure. 1a and b. The increased surface roughness of these octahedra compared with that of original Cu_2O crystals indicates the formation of TiO_2 shells on the core particles (Figure 1c, d). By transmission electron microscopy (TEM) characterization, the uniform coating of TiO_2 thin layers around the whole surface of Cu_2O crystals is clearly evidenced, as shown in Figure 1e and f. Benefitted from the fast exclusive deposition of TiO_2 on Cu_2O crystals, the coated particles are as discrete as original Cu_2O crystals even in the absence of stabilizing agents such as polyvinylpyrrolidone (PVP) or polyelectrolytes. The facile tailoring of $Cu_2O@TiO_2$ core/shell structures attributes to the distinct difference in physicochemical stability between n-type TiO_2 and p-type Cu_2O.[32] The TiO_2 nanocages were also prepared by completely etching out the Cu_2O cores in acidic medium. The sickness of these nanocages is ca. 30 nm (Figure S1). In addition, the nitrogen adsorption-desorption isotherm curves of the TiO_2 nanocages indicate that that the sample has a BET surface area of 63 $m^2\ g^{-1}$. Pore size distribution (PSD) curves (the inset of Figure S2) also demonstrate the existence of mesopores. We believe that such a structural feature brings an additional possibility of interior functionalization by chemical manipulation of the Cu_2O cores inside TiO_2 shells.

Galvanic replacement is a redox process, in which a metal is corroded (sacrificed) by the ions of a second metal when they are in contact in a solution phase.[33,34] This simple reaction can be employed to generate a wide variety of metal nanostructures. Due to much lower redox pair value of Cu_2O/Cu^{2+} (+0.203 V, *vs.* SHE) than that of a noble metal redox pair, such as $AuCl_4^-/Au$ (+1.002 V, *vs.* SHE), $PtCl_6^{2-}/Pt$ (+0.735 V, *vs.* SHE) and $PdCl_4^{2-}/Pd$ (+0.591 V, *vs.* SHE), the Cu_2O crystals can be potentially used as the sacrificial templates for the synthesis of hollow noble metal cages.[35] The galvanic reaction between $Cu_2O@TiO_2$ and metal ions was performed immediately when the solution of $HAuCl_4$

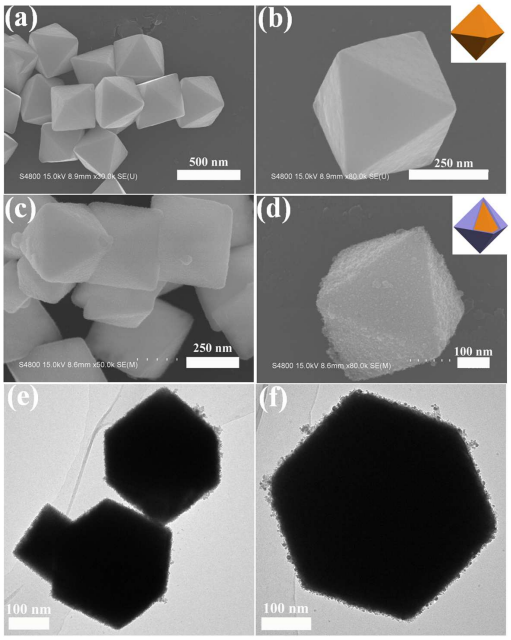

Figure 1. SEM images of (a, b) Cu_2O octahedral with an average edge length of 250 nm and (c, d) octahedral $Cu_2O@TiO_2$ core/shell structures; (e, f) TEM images of $Cu_2O@TiO_2$ structures.

was added into the mixture of $Cu_2O@TiO_2$ and PVP.[20] The solution color changed from carmine to black after the addition of noble metal precursors, indicating the Au ions were reduced quickly. Following the Cu_2O cores being dissolved in HNO_3 solution, $Au@TiO_2$ double-shelled nanocages with octahedral morphologies inherited from the Cu_2O templates are obtained. The obvious red shift of the SPR peak from 560 nm to 580 nm can be observed clearly between Au nanocages and $Au@TiO_2$ double-shelled nanocages because of the large local refractive index of TiO_2 shell encapsulating the Au shell. (Figure S3), which are similar to those in previous work.[36]

The typical structural morphology of the $Au@TiO_2$ double-shelled octahedral nanocages were observed by SEM and TEM (Figure 2a-c). The product mainly consists of well-defined octahedral cages with edge sizes of 250 nm (Figure 2a), indicative of a well-assembled structure without phase separation. The morphologies of the Cu_2O octahedral-shapes were kept very well after the galvanic reactions. Although the thickness of the TiO_2 shell is only near 30 nm, some core-shell structure cages which are demonstrated by the partial dissolution induced by interfacial reactions can even be found in our SEM image (Figure 2b). A closer observation of one cracked nanocage reveals that the cage is composed of abundant nanograins (Figure S4). The SEM images of Au nanocage (Figure S5 and Figure S9) also show clear nanograins, which are in agreement with the literature.[9,35,37] It is considered that these nanograins have joined together to form a solid facet of the Au shell (Figure S5). Meanwhile, mesopores or cavities form into the cage wall, which is further demonstrated by the nitrogen adsorption-desorption isotherm curves (Figure S6). The hollow interior and geometrical structure of as-obtained $Au@TiO_2$ double-shelled nanocages are directly elucidated by TEM, as shown in Figure 2c. In agreement with the SEM findings, the nanocages show a clear hollow interior and high uniformity. A strong contrast difference among

the outer edges (light dark) and inner edges (dark) and center (bright) implies that the octahedral nanocages have two walls of which thickness are all around tens of nanometers. The crystal structure of the obtained product was examined by means of X-ray diffraction (XRD). Figure S7 presents the XRD pattern of the as-synthesized Au@TiO_2 double-shelled nanostructure. The diffraction peaks at about 38.2°, 44.4°, 64.56°, 77.5° can be indexed to the (111), (200), (220), (311) crystal faces of face-centered cubic Au (JCPDS file: 89-3697). The signal at 69.139° comes from the silicon chip. However, the diffraction peaks of TiO_2 are hardly ever observed owing to very low crystallinity of TiO_2 NGs,[38] which agrees with High resolution TEM (HRTEM) image of Au@TiO_2 double-shelled nanocage. (Figure S8).

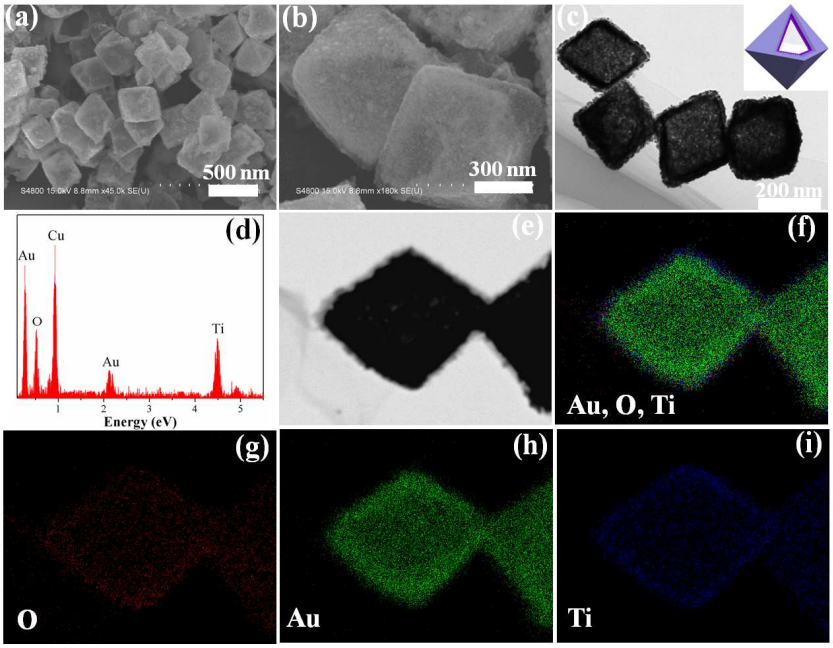

Figure 2. SEM images (a, b) and TEM image(c) of octahedral Au@TiO_2 double-shelled nanocages. (d) EDX spectrum, in which the Cu signal is originated from the copper grid; STEM images (e) and elemental maps (f-i) for mixed, Au, O, Ti, respectively of the octahedral Au@TiO_2 double-shelled nanocages.

In addition, we also applied energy dispersive X-ray spectroscopy (EDX) and X-ray element mapping analysis to further characterize the structure phase and composition of the Au@TiO_2 double-shell nanocages. The elemental compositions of the octahedron nanocages were measured by EDX and shown in Figure 2d suggesting that the products contain Au, Ti and O elements, with the atomic ratio of Ti to O being approximately 1:2. This is consistent with the EDX mapping analysis, which means the samples are a hybrid of TiO_2 and Au. The signal for copper comes from the copper grid. Figure 2e-i show representative STEM images of hollow Au@TiO_2 double-shelled octahedrons and the corresponding Au, Ti, and O elemental maps, from which we can clearly see that the Au hollow nanocages are covered with a shell assembled from TiO_2 NGs. These results conclusively show that uniform core-shell Au@TiO_2 double-shelled nanocages were synthesized. The TiO_2 shell has nanospaces between the TiO_2 NGs enabling the access of reactants to the Au shell and the mesopores between the Au nanograins also allow the reactants entering into the cavity easily.

To investigate the influence of the concentration of $HAuCl_4$ to the morphological evolution of Au@TiO_2 double-shelled nanocages, the Cu_2O@TiO_2 core-shell octahedra was titrated with 5, 10, 20 and 30 mM of the solution of $HAuCl_4$ (1.5 mL). The TEM images reveal that small Au nanoparticles inside the TiO_2 shell present at a small proportion of $HAuCl_4$ (Figure 3a). The clear Au@TiO_2 hollow shell was formed with the introduction of more $HAuCl_4$ (Figure 3b). When the titrated volume of $HAuCl_4$ solution reached 20 mM, the interior of the Au@TiO_2 double-shelled became blacker indicating the Au shell became thicker (Figure 3c). When increasing the concentration of $HAuCl_4$ to 30 mM, no intact Au shell was observed, leaving disordered aggregation of small particles inside the TiO_2 shell (Figure 3d). This result demonstrates that intact Au@TiO_2 double-shelled octahedra can form at a certain amount of $HAuCl_4$. If excessive $HAuCl_4$ was added into the reaction, the Au shell would collapse. Figure 3 shows a schematic illustration and electron microscopy images of the nanostructures at different stages. When an aqueous $HAuCl_4$ solution is added into an aqueous suspension of Cu_2O nanoparticles, galvanic replacement will be initiated immediately. As a result, Cu^+ atoms will be oxidized and dissolved into the solution, generating a small hole on the surface of the nanoparticles. At the same time, the electrons will quickly migrate to the surface of the nanoparticles and be captured by $AuCl_4^-$ to generate Au atoms via a reduction reaction. The newly formed Au atoms tend to be deposited epitaxially on the surface of the Cu_2O nanoparticle. Due to very small amount of $HAuCl_4$ added into the system, only some Au nanoparticles present inside the TiO_2 shell when the inner Cu_2O cores were dissolved by acid. When more $HAuCl_4$ (10 mM and 20 mM) is added, an intact Au shell formed through further dissolution of Cu_2O. However, if more $HAuCl_4$ is added into the reaction system, the $AuCl_4^-$ will cause dealloying for the Au-

Cu_2O shells by selectively removing Cu_2O atoms from the Au-Cu_2O shells, thus generating hollow nanocages with biger holes and causing collaps.[33] In this case, the addition of PVP was very important when $HAuCl_4$ was added into the solution. The gold shell structure tends to collapse and the final product is composed purely of gold particles without PVP. It is considered that the PVP polymer molecules can absorb on the surface of the gold nanograins and play the role as bridges connecting the adjacent nanograins together, thus keeping the octahedral shape of the gold shells.[29]

The catalytic activity of the as-prepared Au@TiO_2 double-shelled structures was evaluated through the reduction of 4-NP in the presence of an excess amount of $NaBH_4$, which has been widely used as a model reaction for evaluating the catalytic activity of various

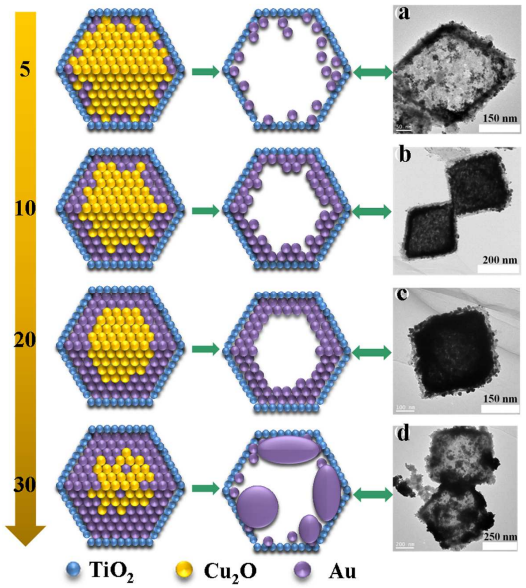

Figure 3. Schematic illustration and TEM images of Au@TiO_2 samples obtained at four different stages of the galvanic replacement reaction, in which the Cu_2O@TiO_2 was titrated with (a) 5 mM, (b) 10 mM, (c) 20 mM, (d) 30 mM $HAuCl_4$ (1.5 mL).

metal NPs. As observed in Figure 4a, it is well known that 4-NP solution exhibits a strong absorption peak at 317 nm which is remarkably red-shifted to 400 nm when treated with an aqueous solution of $NaBH_4$.[39-41] The absorption at 400 nm comes from the formation of 4-nitrophenolate ion owing to an increase in solution alkalinity upon the addition of $NaBH_4$.[42] It was demonstrated that the reduction reaction did not proceed without catalysts, in the absence of Au@TiO_2 catalysts, the peak at 400 nm stayed unchanged for over 100 min (Figure 4b). To highlight the excellent catalytic activity, we also prepared Au nanocages using octahedral Cu_2O template, which also shows the typical morphologies for octahedral Au nanocages by means of the similar reduction processes as Au@TiO_2 double-shelled octahedral nanocages (Figure S9). Au NPs@TiO_2 double-shelled nanocages (Figure S10) and Au NPs (Figure S11) were synthesized, which are similar with Au@TiO_2 double-shelled nanocages and Au nanocages except for the absence of PVP. To demonstrate unique properties of octahedral structure and synergistic effects between the Au and TiO_2 shells for improvement of catalytic activities, Au content of all the samples measured by the ICP is consistent in performance measurement (Table S1). The catalytic activities of the Au@TiO_2 double-shelled nanocages, Au nanocages, Au NP@TiO_2 nanocages and Au NPs catalysts were compared in the reaction of 4-NP reduction (Figure 4c, d, e, f). After the catalyst was added, the absorption peak at 400 nm gradually dropped in intensity as the reduction reaction proceeded. At the same time, with the production of 4-AP, a new absorption peak started to appear as a shoulder at 300 nm, which indicated the reduction of 4-NP to 4-AP.[43-45] It was worthwhile to note that the reduction started immediately after the addition of the catalyst and there was no induction time required. This might be advantageous for ease of use in real technological applications. The reduction kinetics could be monitored by performing spectroscopic measurements based on the colour changes that were involved in the reaction.[46,47] From the UV-visible absorption spectra in Figure 4c, it took 5 min for Au@TiO_2 double-shelled nanocages to complete the catalytic reaction which exhibited excellent catalytic performance. For the other catalysts (Figure 4d, e, f), the reaction time was different from each other. As observed in Figure 5f, it took 12 min for the Au NPs to completely catalyze the reaction, which demonstrated that the catalytic activity of Au NPs was obviously lower. However, for Au NPs@TiO_2 nanocages (Figure 4e), the reaction time of which was shorter than of the Au NPs but longer than of the Au nanocages (Figure 4d). The reduction rates show that the 4-NP can be completely reduced and all catalysts exhibit catalytic performance. Especially, Au@TiO_2 double-shelled nanocages catalyst shows the best catalytic performance.

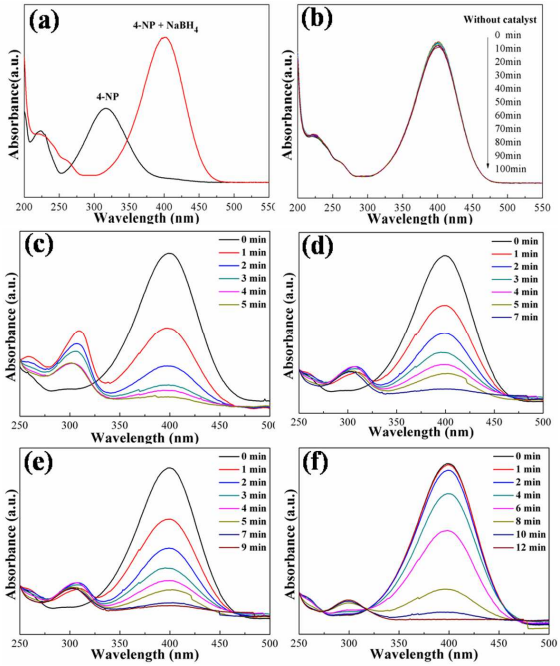

Figure 4. (a) UV-visible absorption spectra of a solution of 4-NP with and without $NaBH_4$. (b) Time-dependent UV-visible absorption spectra for the reduction of 4-NP with $NaBH_4$, but without Au@TiO_2 catalyst. (c-f) UV-visible spectra showing the reduction of 4-NP to 4-AP on Au@TiO_2 double-shelled nanocages, Au nanocages, Au NPs@TiO_2 nanocages and Au NPs catalysts.

The kinetic analysis of these reactions can be carried out as described from the temporal decay of these peaks. Time-dependences of the absorbance at 400 nm for the reduction of 4-nitrophenol on Au@TiO_2 double-shelled nanocages, Au nanocages, Au NPs@TiO_2 nanocages and Au NPs indicate that all the catalysts exhibit catalytic performance and 4-NP can be completely reduced to 4-AP within 12 min (Figure 5a). The linear relation of $\ln(C_t/C_0)$ versus reaction time indicates that the reactions followed first order kinetics.[48,49] The apparent rate constants (k) were estimated from diffusion-coupled first order reaction kinetics using the slopes of straight lines in Figure 5b. The rate constant k which was calculated using the rate equation $\ln(C_t/C_0) = kt$ is 1.35×10^{-2} s^{-1}, 9.5×10^{-3} s^{-1}, 8.03×10^{-3} s^{-1}, 4.93×10^{-3} s^{-1} for Au@TiO_2 double-shelled nanocages, Au nanocages, Au NPs@TiO_2 nanocages and Au NPs catalysts, respectively. We also calculated the TOFs of various catalysts (Table S1). The TOFs can reach 870, 621, 483 and 360 h^{-1} for Au@TiO_2 double-shelled nanocages, Au nanocages, Au NPs@TiO_2 nanocages and Au NPs catalysts, respectively. Au@TiO_2 double-shelled nanocages and Au nanocages show better catalytic performance than Au NPs@TiO_2 nanocages and Au NPs. The catalytic stability tests of Au@TiO_2 double-shelled nanocages and Au nanocages are shown in Figure 5c-d. The Au@TiO_2 double-shelled nanocages catalyst could be successfully reused for ten reaction cycles with a conversion efficiency of more than 90%, indicating that Au@TiO_2 double-shelled nanocages catalyst is stable and efficient. However, Au nanocages display relatively poor stability and reusability. The catalytic activity of Au@TiO_2 double-shelled nanocages remained almost constant after ten cycles and only a little lower after the tenth cycle (Table S2). But it should be noted that the k value was still high and reached 1.07×10^{-2} s^{-1} after the tenth cycle, which confirmed that the catalyst possessed good stability and reusability. The decrease in k value may be attributed to the loss of catalyst arising from separation and purification process.[50]

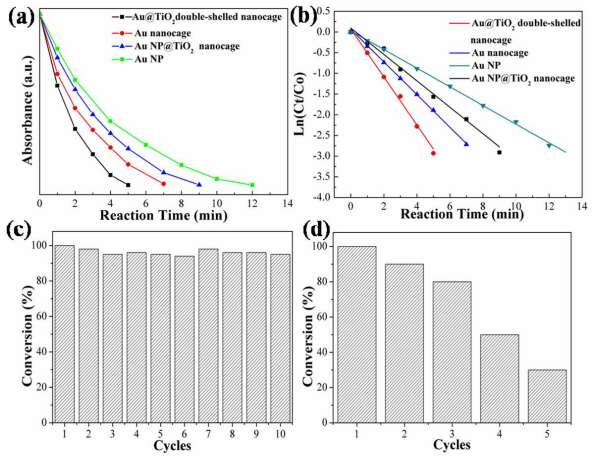

Figure 5. (a) Time-dependences of the absorbance at 400 nm for the reduction of 4-nitrophenol on Au@TiO_2 double-shelled nanocage, Au nanocage, Au NPs@TiO_2 nanocage and Au NPs; (b) plots of $\ln(C_t/C_0)$ against the reaction time of Au@TiO_2 double-shelled nanocages, Au nanocages, Au NPs@TiO_2 nanocages and Au NPs. (c and d) the catalytic stability tests of Au@TiO_2 double-shelled nanocages and Au nanocages.

These results suggest that Au@TiO_2 double-shelled nanocages show better catalytic activity and stability than the corresponding Au nanocages, Au NPs@TiO_2 nanocages and Au NPs due to their unique structures. First, the interface between the TiO_2 NGs and Au nanograins favors the fast diffusion of reactants and products.[21,38] Second, the hollow structure of Au@TiO_2 double-shelled nanocages catalysts leads to confinement of the reactants into the inner space, resulting in the higher instantaneous concentration of reactants and products in the nanoreactors providing a driving force to accelerate the catalytic reaction.[28] Third, Au@TiO_2 double-shelled nanocages catalysts have many corners and edges on which atoms have unsaturated valency with less number of bonds around them than those in the interiors or on the faces, largely improving the catalytic activity.[49] Forth, the synergistic effect between the Au nanowall and the TiO_2 shells will speed up the rate of charge transfer and effectively inhibit catalyst poisoning, accelerating the reduction of 4-NP to 4-AP.[36,38] Finally, the TiO_2 shell can restrict the Au nanocages from exposing to the reactants and the surrounding medium and protect the Au nanocages, thus improving the catalytic stability.[36,38]

4. Conclusions

In conclusion, we have synthesized nano-sized Au@TiO_2 hollow octahedral hetero-structured nanocages composed of a hollow interior and double porous shells with Au shell inside and TiO_2 shell outside. The Au@TiO_2 double-shelled nanocages was readily obtained by depositing uniform TiO_2 shells on Cu_2O octahedra and then using Cu_2O as sacrificial templates to form Cu_2O@Au@TiO_2 core/double-shell structures. Au@TiO_2 double-shelled nanocages were fabricated by treating the Cu_2O@Au@TiO_2 structures in diluted HNO_3, involving the process of removal of the Cu_2O core. We found that the nanocages show unique structural features such as octahedral shape, porous shells, uniform coating of TiO_2 NGs, enhanced synergistic effects and decreased leaching of noble metals leading to extremely high catalytic activity for reduction of 4-nitrophenol with the apparent rate constants k of 1.35×10^{-2} s^{-1} and TOF of 870 h^{-1}. The catalytic stability is also superior with the conversion remaining over 90% even after ten cycles of catalytic reaction. Most importantly, this method will open up a new way to synthesize a variety of hybrid metal-oxide hollow nanocages.

Acknowledgements

This work was supported by the National Natural Science Foundation of China (21236003, 21206042, 20925621, and 21176083), the Basic Research Program of Shanghai (13NM1400700, 13NM1400701), and the Fundamental Research Funds for the Central Universities.

Notes and references

Key Laboratory for Ultrafine Materials of Ministry of Education, School of Materials Science and Engineering, East China University of Science and Technology, Shanghai 200237, China. E-mail: yhzhu@ecust.edu.cn; czli@ecust.edu.cn. Fax: +86 21 6425 0624; Tel: +86 21 6425 2022.

† Electronic Supplementary Information (ESI) available: additional Figures as noted in the text. See DOI: 10.1039/b000000x/

1. K. An, T. Hyeon, *Nano Today*, 2009, **4**, 359.
2. J. Liu, H. Q. Yang, F. Kleitz, Z. G. Chen, T. Yang, E. Strounina, G. Q. Lu and S. Z. Qiao, *Adv. Funct. Mater*., 2012, **22**, 591.
3. Q. Zhang, W. Wang, J. Goebl and Y. Yin, *Nano Today*, 2009, **4**, 494.
4. Z. Wang, X. W. Lou, Adv. Mater., 2008, **20**, 3987.

5. S. E. Skrabalak, J. Chen, Y. Sun, X. Lu, L, Au, C. M. Cobley and Y. Xia, *Acc. Chem. Res*., 2008, **41**, 1587.
6. O. Shchepelina, V. Kozlovskaya, S. Singamaneni, E. Kharlampieva and V. V. Tsukruk, *J. Mater. Chem*., 2010, **20**, 6587.
7. Z. Wang, L. Zhou and X. W. Lou, *Adv. Mater*., 2012, **24**, 1903.
8. S. C. Glotzer, M. J. Solomon, *Nat. Mater*., 2007, **6**, 557.
9. J. Fang, S. Lebedkin, S. Yang and H. Hahn, *Chem. Commun*., 2011, **47**, 5157.
10. J. Chen, M. Yang, Q. Zhang, E. C. Cho, C. M. Cobley, C. Kim, C. Glaus, L. V. Wang, M. J. Welch and Y. Xia, *Adv. Funct. Mater*., 2010, **20**, 3684.
11. M. A. Mahmoud, R. Narayanan and M. A. El-sayed, *Acc. Chem. Res*., 2013, **46**, 1795.
12. Z. M. Peng, J. B. Wu and H. Yang, *Chem. Mater*., 2010, **22**, 1099.
13. Z. M. Peng, H. J. You, J. B. Wu and H. Yang, *Nano Lett*., 2010, **10**, 1492.
14. H. P. Liang, H. M. Zhang, J. S. Hu, Y. G. Guo, L. J. Wan and C. L. Bai, *Angew. Chem. Int. Ed*., 2004, **43**, 1540.
15. Y. G. Sun, Y. N. Xia. *Science*, 2002, **298**, 2177.
16. G. X. Zhang, S. H. Sun, R. Y. Li and X. L. Sun, *Chem. Eur. J*., 2010, **16**, 10630.
17. D. Seo, H. Song, *J. Am. Chem. Soc*., 2009, **131**, 18210.
18. X. Q. Huang, H. H. Zhang, C. Y. Guo, Z. Y. Zhou and N. F. Zheng, *Angew. Chem. Int. Ed*., 2009, **48**, 4808.
19. Z. H. Lin, M. H. Lin and H. T. Chang, *Chem. Eur. J*., 2009, **15**, 4656.
20. H. Feng, S. Sun, H. You, S. Yang, J. Fang, S. Guo, Z. Yang, B. Ding and X. Song, *Cryst. Growth. Des*., 2011, **11**, 3694.
21. J. Fang, S. Liu and Z. Li, *Biomaterials*, 2011, **32**, 4877.
22. A. Corma and H. Garcia, *Chem. Soc. Rev*., 2008, **37**, 2096.
23. T. Yang, J. Liu, Y. Zheng, M. J. Monteiro and S. Z. Qiao, *Chem. Eur. J*., 2013, **19**, 6942.
24. F. Xiao, *Chem. Commun*., 2012, **48**, 6538.
25. I. Lee, J. B. Joo, Y. Yin and F. Zaera, *Angew. Chem. Int. Ed*., 2011, **123**, 10390
26. J. Liu, S. Z. Qiao, J. S. Chen, X. W. Lou, X. Xing and G. Q. Lu, *Chem. Commun*., 2011, **47**, 12578.
27. R. Guttel, M. Paul and F. Schuth, *Chem. Commun*., 2010, **46**, 895.
28. B. Liu, S. Yu, Q. Wang, W. Hu, P. Jing, Y. Liu, W. Jia, Y. Liu, L. Liu and J. Zhang, *Chem. Commun*., 2013, **49**, 3757.
29. Q. Yao, R. Che, C. Liang, J. Zhang and Z. Wen, *J. Mater. Chem*., 2011, **21**, 3960.
30. J. Yang, D. Shen, L. Zhou, W. Li, X. Li, C. Yao, R. Wang, A. M. El-Toni, F. Zhang and D. Zhao, *Chem. Mater*., 2013, **25**, 3030.
31. B. N. Khlebtsov, V. A. Khanadeev, E. V. Panfilova, O. A. Inozemtseva, A. M. Burov and N. G. Khlebtsov, *J. Quant. Spectrosc. Ra*., 2013, **121**, 24.
32. Z. Wang and X. W. Lou, *Adv. Mater*., 2012, **24**, 4124.
33. X. Xia, Y. Wang, A. Ruditskiy and Y. Xia, *Adv. Mater*., 2013, **25**, 6325.
34. J. Pal, M. Ganguly, S. Dutta, C. Mondal, Y. Negishi and T. Pal, *CrystEngComm*, 2014, **16**, 883.
35. S. Sun and Z. Yang, *Chem. Commun*., 2014, **50**, 7403.
36. Z. W. Seh, S. Liu, S. -Y. Zhang, K. W. Shah and M. -Y. Han, *Chem. Commun*., 2011, **47**, 6689.
37. S. E. Skrabalak, J. Chen, Y. Sun, X. Lu, L. Au, C. M. Cobley and Y. Xia, *Acc. Chem. Res*., 2008, **41**, 1587.
38. L. Han, C. Zhu, P. Hu and S. Dong, *RSC Adv*., 2013, **3**, 12568.
39. Y. Y. Lin, Y. Qiao, Y. J. Wang, Y. Yan and J. B. Huang, *J. Mater. Chem*., 2012, **22**, 18314.
40. S. Sarkar, A. K. Sinha, M. Pradhan, M. Basu, Y. Negishi and T. Pal, *J. Phys. Chem. C*, 2011, **115**, 1659.
41. L. H. Ai, H. T. Yue and J. Jiang, *J. Mater. Chem*., 2012, **22**, 23447.
42. K. Layek, M. L. Kantam, M. Shirai, D. N. Hamane, T. Sasaki and H. Maheswaran, *Green Chem*., 2012, **14**, 3164.
43. B. C. Liu, S. L. Yu, Q. Wang, W. T. Hu, P. Jing, Y. Liu, W. J. Jia, Y. X. Liu, L. X. Liu and J. Zhang, *Chem. Commun*., 2013, **49**, 3757.
44. S. C. Tang, S. Vongehr and X. K. Meng, *J. Mater. Chem*., 2010, **20**, 5436.
45. X. Zhang and Z. H. Su, *Adv. Mater*., 2012, **24**, 4574.
46. Y. H. Zhu, J. H. Shen, K. F. Zhou, C. Chen, X. L. Yang and C. Z. Li, *J. Phys. Chem. C*, 2011, **115**, 1614.
47. H. L. Jiang, T. Akita, T. Ishida, M. Haruta and Q. Xu, *J. Am. Chem. Soc*., 2011, **133**, 1304.
48. Q. An, M. Yu, Y. Zhang, W. Ma, J. Guo and C. Wang, *J. Phys. Chem. C*, 2012, **116**, 22432.
49. M. A. Mahmoud, C. E. Tabor, M. A. El-sayed, Y. Ding and Z. L. Wang, *J. Am. Chem. Soc*., 2008, **130**, 4590.
50. X. Yang, H. Zhong, Y. Zhu, H. Jiang, J. Shen, J. Huang and C. Li, *J. Mater. Chem. A*, 2014, **2,** 9040.